Climatic Change (2021) 164:25
https://doi.org/10.1007/s10584-021-02980-x

Future projection of maximum potential storm surge height at three major bays in Japan using the maximum potential intensity of a tropical cyclone

Nobuhito Mori[1] · **Nozomi Ariyoshi**[2] · **Tomoya Shimura**[1] · **Takuya Miyashita**[1] · **Junichi Ninomiya**[3]

Received: 30 June 2020 / Accepted: 6 January 2021 / Published online: 01 February 2021

Abstract
This study developed an integrated model for the long-term assessment of extreme storm surge heights based on the maximum potential intensity (MPI) of a tropical cyclone, which is used to conduct future climatological projections of maximum potential storm surge height (MPS). We apply the MPS method to three major bays in Japan, Tokyo, Osaka, and Nagoya, using two mega-ensemble climate change projections: CMIP5 and d4PDF. The sensitivity of MPS change relative to sea surface temperature (SST) change for three major bays in Japan is about 0.12 m/°C during tropical cyclone season, which is about 1/10 of the change when considering SST rise only. Both the mean and variance of future MPS values will be much greater, especially in September and under higher representative concentration pathway (RCP) scenarios.

Keywords Extreme storm surge · Maximum potential intensity · Tropical cyclone · Climate change · Future change

✉ Nobuhito Mori
mori@oceanwave.jp

Tomoya Shimura
shimura.tomoya.2v@kyoto-u.ac.jp

Takuya Miyashita
miyashita.takuya.4w@kyoto-u.ac.jp

Junichi Ninomiya
jnino@se.kanazawa-u.ac.jp

[1] Disaster Prevention Research Institute, Kyoto University, Uji, Kyoto, 611-0011, Japan

[2] Graduate School of Engineering, Kyoto University, Uji, Kyoto, 611-0011, Japan

[3] Faculty of Geosciences and Civil Engineering, Kanazawa University, Kakuma-machi, Kanazawa, 920-1192, Japan

1 Introduction

Extreme tropical cyclones (TCs) and their related storm surges have been observed worldwide over the last few decades. Some disastrous TCs have produced catastrophic storm surges, including Hurricane Katrina in 2005, Cyclone Nargis in 2008, Typhoon Morakot in 2009, Hurricane Sandy in 2012, Typhoon Haiyan in 2013, Cyclone Pam in 2015, Hurricanes Irma and Maria in 2017, Typhoon Jebi in 2018, and Typhoon Hagibis in 2019. For example, Typhoon Haiyan was an extremely intense TC that struck the Philippines in November 2013, causing catastrophic damage with casualties numbering more than 6000. TC Haiyan is the most powerful TC to make landfall to date (Schiermeier 2013). The minimum central pressure of TC Haiyan was 895 hPa, and the storm surge in the Gulf of Leyte was over 5 m (Mori et al. 2014). The large area was inundated and the inundation was the major cause of causalities by TC Haiyan. Typhoon Jebi in 2018 yielded large-scale inundation in Osaka Bay, Japan, and Kansai-Osaka International Airport was completely inundated and resulted in 2 billion USD damage to the airport (Mori et al. 2019b). Storm surge events like these are not frequent, but once these disasters occur, they result in catastrophic loss of human life and infrastructure.

Global warming is expected to affect the characteristics of TCs, namely the frequency, intensity, and track. The Intergovernmental Panel on Climate Change (IPCC) qualitatively discussed that genesis number of TCs overall will be fewer but intensity will be stronger over the globe in the Fifth Assessment Report (AR5) IPCC (2013) and the Special Report on the Ocean and Cryosphere (SROCC; Pörtner et al. (2019)). Specifically, by the end of the twenty-first century, the number of intense tropical cyclones is expected to increase from present day values as a result of climate change (e.g., Bender et al. (2010), Knutson et al. (2010), Emanuel (2013), and Yoshida et al. (2017)). Future changes in TC characteristics, however, are uncertain over both regional and global scales due to performance of climate models and insufficient number of TC events at particular locations.

TC-related natural hazard risk assessments are required to develop adaptation measures that depend on global warming (e.g., Mori and Takemi (2016)). Additionally, both the intensity and frequency of extreme events are important to project in advance, so disaster planning can consider both hard and soft countermeasures against extreme hazards. Therefore, assessing extreme storm surges in a future climate is important to develop adaptation strategies. However, the number of observed historical events of extreme storm surge is extremely limited (typically one or two extreme events per 50–100 years at a particular location), and quantitative evaluation of extreme storm surge is difficult when using historical events alone using extreme value analysis. Therefore, we need to augment the historical dataset to help understand the long-term effects of climate change on TC intensity and storm surge.

To assess the uncertainty in projecting future changes in storm surge, the small dataset was augmented with an ensemble projection (typically 20–25-year time-slice experiments). The straightforward approach for the storm surge assessment is using a dynamic storm surge model (e.g., nonlinear shallow water equation) forced by sea surface pressure and winds from a global climate model (GCM) (Yasuda et al. 2016; Bloemendaal et al. 2019; Lin et al. 2019). The use of dynamic storm surge model with GCM forcings is quite accurate if the accuracy of sea surface pressure and winds by GCMs is reasonable. On the other hands, the results highly depend on the performance of GCMs which has large uncertainty resolving TCs due to resolution of GCMs, cumulus schemes, and etc. Additionally, the time-slice experiment of climate projection is generally performed over 20–25 years for both present and future climate conditions. However, the extreme storm surge occurs at intervals greater

than 10 years generally. Therefore, it is difficult to discuss with extreme storm surge height longer than period of time-slice experiments generally. The computational load is still a major obstacle to handle such a large computation cost due to fine resolution of storm surge modeling (Δx <1 km). A statistical model is useful for long-term assessment of storm surge due to low computational cost. For example,. Irish et al. (2009) used empirical estimation maximum surge as a function of minimum central pressure and distance between target location and TC center. Their simple statistical model is useful for climate application but large number of computation by dynamic storm surge model is necessary to adjust the model coefficients. Furthermore, the large number of synthetic TCs can be obtained by statistical tropical cyclone model (e.g., Nakajo et al. (2014)). However, the statistical tropical cyclone model has difficulty to consider climate change in the model. The extension of time integration of GCM can increase number of extreme events and large ensemble climate projection experiment using a single GCM has been conducted in several projects. The copious results of more than 5000 years of climate projections are beginning to be used for global warming impact assessment on extreme storm surge (Mori et al. 2019a) but TC intensity bias is still there. In general, dynamic and statistical methods have been used to calculate storm surge heights for the long-term assessment of storm surge hazard but there are several limitations depend on the approaches. Reducing computational cost, including uncertainty of the climate projection and avoiding GCM bias for TCs need to improve for extreme storm surge projection in climate research.

Based on this background, we developed a method for seamlessly estimating the maximum potential storm surge height (MPS) from the climate values of the GCM by applying the theory of maximum potential intensity (MPI) of a TC Emanuel (1988). The use of MPI is alternative approaches using environmental factors (monthly sea surface temperature and etc) which are more reliable in the climate projections. It also can reduce computational costs. First, the MPI of a TC is calculated from the monthly mean climate field. Then, the formula to estimate the maximum potential storm surge anomaly is derived considering the cross-sectional topography of each bay. In addition, we calculate the MPS for three major Japanese bays using the MPI barometric pressure and sea surface wind speed as inputs to investigate future changes in extreme storm surge water heights and the effects of global warming on these values.

2 Methodology

2.1 Estimation of maximum TC intensity

The aim of this study is to estimate the maximum potential storm surge height (MPS) based on the MPI. Here, the maximum potential means the estimated maximum given the environment. We here define "maximum potential" as an idealized maximum value from the environment factors (or climatic conditions) neglecting time-series and other detail of dynamic mechanisms. The primary reason for this approach is the difficulty of estimating maximum values with low-frequency events, such as when an intense TC makes landfall at a particular location and determining the extreme storm surge at that location. For example, the number of TCs that make landfall in Japan is 2–3/year on average, and the occurrence of severe storm surges is less than that amount due to sensitivity to wind-induced surge, tracks, and other factors. Therefore, a large ensemble set is necessary to estimate the probability of the storm surge height at a particular location. Furthermore, estimating the maximum of storm surge height is more difficult when compared to estimating the probability of the

maximum height. On the other hand, the climatological environment (e.g., monthly sea surface temperature (SST) or air temperature) is stable and validated in detail, and therefore use of environmental factors to explain extremes is an alternative approach to process based model.

Here we estimate the maximum potential TC intensity as well as the maximum potential storm surge height from climatological environmental factors. There are several theories and empirical formulas to estimate maximum potential TC intensity (e.g., Balaguru et al. (2016)). We choose MPI by Emanuel (1988) which is parameterized SST and convective available potential energy. The main reason is implementation of changes in SST and atmospheric stability change in the future climate. We assume the worst case TC to generate MPS for given minimum pressure and maximum wind speed which is defined by maximum potential storm surge heights in this study. The flow of evaluating the climatic MPS via the climatic MPI of the TC is presented in Fig. 1. The modeling is divided into two parts as follows.

1. Estimate MPI and maximum potential wind speed using climate conditions
2. Estimate MPS using MPI and maximum potential wind speed.

We estimate MPI as well as MPS from climatological environment factors to avoid dynamic modeling of TCs and storm surges. Each computational process is explained in the Supplemental Material A.1.

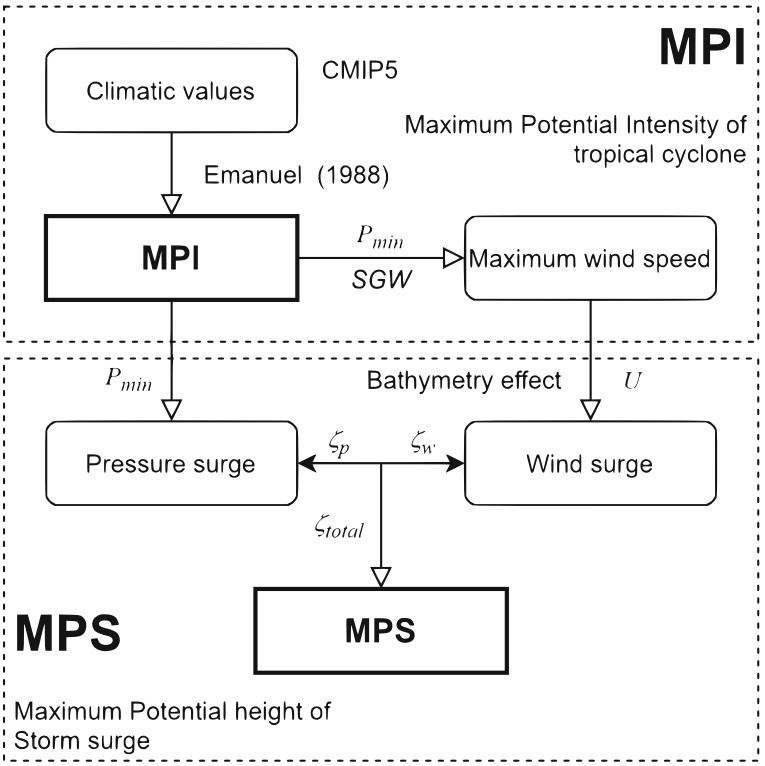

Fig. 1 Outline of maximum potential surge height (MPS) estimation

2.2 Estimation of maximum storm surge height

The next step is to estimate the maximum storm surge height from the given pressure and wind speed. Storm surge is caused by the suction effect of lower air pressure coupled with the effect of direct wind stress on the sea surface. We assume both effects are independent of each other and can be semi-analytically evaluated using a one-dimensional, axial cross-section of the bay for simplification as follows.

If the sea surface height change is statically proportional to the barometric pressure change, the sea surface height for the barometric pressure drop in ΔP is expressed by the following equation:

$$\zeta_p = \frac{\Delta P}{\rho_w g}. \tag{1}$$

where ζ_p is the pressure-induced surge, ρ_w is the sea water density, and g is the gravitational acceleration. Equation 1 gives a 1-cm sea surface rise for a 1-hPa decrease of atmospheric pressure, approximately. The pressure-induced surge can be expressed by Eq. 1 for most situations, but there is a resonance of pressure waves and long waves in the bay. The pressure-induced surge including resonant effect can be maximized when the TC translation speed V_T is equal to the long wave celerity C in the bay (i.e., Proudman resonance; Proudman, 1929). We consider the maximum pressure-induced surge considering resonant condition explained in the Supplemental Material A.2.

The wind-induced surge is maximized when the TC approaches the target bay along the worst case storm track. The wind-induced surge is the dominant part of an extreme storm surge, and numerical modeling is necessary to estimate the time-dependent process of the wind-induced surge, generally. To estimate the maximum value, we assume a maximum stationary condition such that the TC induces a maximum storm surge. Then, we can neglect the time-dependent term and the lateral advection term from the lwave equation for wind-induced storm surge modeling.

The following static condition balances the difference between the sea surface wind stress τ_s (positive onshore) and the stress due to the bottom sea floor roughness τ_b (positive offshore) with the gradient of the sea surface.

$$\tau_s - \tau_b = \rho_w g \left(h + \zeta_w\right) \frac{d\zeta_w}{dx}, \tag{2}$$

where ζ_w is the wind-induced surge height. Assuming a small ζ_w relative to the water depth h, the sea surface gradient and the stresses become:

$$\frac{d\zeta_w}{dx} = \frac{\tau_s - \tau_b}{\rho_w g h}. \tag{3}$$

Considering the surface stress and bottom stress, Eq. 3 can be rewritten as:

$$\frac{d\zeta_w}{dx} = \frac{\rho_a C_D \left(1 + \lambda\right)}{\rho_w g h} U^2 \tag{4}$$

where C_D is the momentum transfer coefficient from the wind to sea surface and λ is the bottom roughness coefficient. Assuming a constant water depth h and integrating from the bay mouth ($x = 0$) to the coastline $x = L$, we have a simple formula for wind-induced surge ζ_w:

$$\zeta_w = \frac{\rho_a C_D \left(1 + \lambda\right)}{\rho_w g} \cdot \frac{L}{h} \cdot U^2. \tag{5}$$

Since Eq. 5 is too simplified, we will include the real bottom bathymetry. We still assume a one-dimensional channel from offshore to onshore but allow for an arbitrary water depth

along the channel. Then the wind-induced surge height ζ_w is given by the following equation:

$$\frac{d\zeta_w}{dx} = \frac{\rho_a}{\rho_w g} \cdot \frac{K}{h\,(x)} \cdot U^2 \tag{6}$$

where K is a tuning constant for the target bay combining C_D and λ. A numerical integration of the cross-sectional bathymetry from the mouth of the bay to the coastline over the depth of the bay using Eq. 6 gives the spatial distribution of surface height ζ_w that takes into account the influence of the cross-sectional topographic change to some extent. We need to solve Eq. 6 numerically, but it does not have time-dependent variables. Therefore, it is necessary to integrate Eq. 6 excluding wind speed U for a particular bay. The constant K depends on the bathymetry, and it will be validated in the next section.

3 Model validation

3.1 Validation of MPI

First, the MPI results using the CMIP5 model are validated against reanalysis data and modeled TCs using the mega ensemble climate projection data. The CMIP5 projections used in this study are shown in Table 1. Here, the monthly averages of SST, CAPE, and other environmental variables from up to 21 models for the RCP8.5 and RCP2.6 scenarios are presented in Table 1 (19 projections for RC4.5 and 15 projections for RCP6.0), and the monthly averages for the 25 year historical climate (1979–2003) and future climate (2075–2099) with different RCP scenarios are re-meshed in a $2.5 \times 2.5\,^{\circ}$ grid.

To verify the accuracy of the MPI for each model in CMIP5, the MPI reanalysis data was evaluated using monthly mean values of atmospheric information from JRA-55 (Kobayashi

Table 1 List of CMIP5 model for analysis

Model	Historical	RCP2.6	RCP4.5	RCP6.0	RCP8.5
CCSM4	✓	✓	✓	✓	✓
GFDL-CM3	✓	✓	✓	✓	✓
GFDL-ESM2G	✓	✓	✓	✓	✓
GFDL-ESM2M	✓	✓	✓	✓	✓
GISS-E2-H	✓	✓	✓	✓	✓
GISS-E2-R	✓	✓	✓	✓	✓
HadGEM2-AO	✓	✓	✓	✓	✓
HadGEM2-ES	✓	✓	✓	✓	✓
IPSL-CM5A-LR	✓	✓	✓	✓	✓
MIROC5	✓	✓	✓	✓	✓
MRI-CGCM3	✓	✓	✓	✓	✓
CanESM2	✓	✓	✓		✓
CNRM-CM5	✓	✓	✓		✓
MPI-ESM-LR	✓	✓	✓		✓
MPI-ESM-MR	✓	✓	✓		✓
IPSL-CM5A-MR	✓	✓			✓
total	16	16	15	11	16

et al. 2015) and SST from COBE-SST (Ishii et al. 2005), respectively. The Taylor diagram for the MPI from the CMIP5 models and JRA-55 during TC seasons is shown in Fig. A.3. Figure A.3a shows the results for tropical regions in the Western North Pacific (WNP) and (b) shows the results for the TC development region (i.e., middle latitude) (10–35° N) in the WNP. For example, CCSM4 in Fig. A.3a shows a standard deviation of 42.1, an RMSE of 12.5, and a correlation coefficient of 0.96, which is close to that for JRA-55. The correlation coefficients of several models are less than 0.9 in the tropics. On the other hand, both the correlation coefficients and standard deviations are widely spread in the TC development region as shown in Fig. A.3b. Five models with correlation coefficients less than 0.8 (FGOALS-s2, MIROC-ESM, MIROC-ESM-CHEM, NorESM1-M, and NorESM1-ME) have standard deviations that are about 10 less than the 26.0 value from JRA-55. Based on the validation of the MPI with JRA-55 reanalysis, those five models are excluded from this analysis. Therefore, our study includes 16 models from the RCP8.5 and RCP2.6 scenarios, 11 models from RCP6.0, and 15 models from RCP4.5.

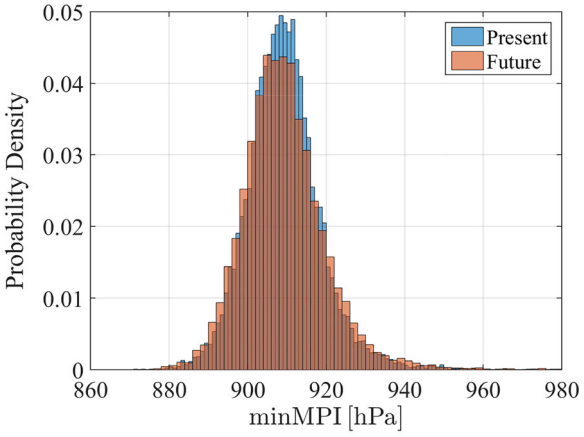

(a) PDF of minimum MPI along the TC tracks

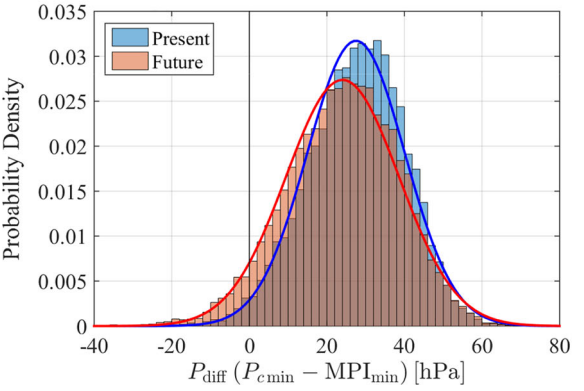

(b) Difference between minimum central pressure of modeled TC and minimum MPI along the TC tracks

Fig. 2 Relation between minimum central pressure of modeled TC, P_{min} and the minimum MPI, MPI_{min} along the track (blue: present climate, red:+4K climate)

The next validation compared MPI results with TCs modeled using the GCM. This step reveals how the MPI gives the maximum TC intensity for a climatological environment. The number of extreme events, especially TCs, from the CMIP5 time-slice experiment is insufficient to discuss statistically. The large number of climate ensembles is needed to validate statistical relations between MPI with modeled TCs in the GCM. The mega ensemble experiments, the so-called d4PDF (Mizuta et al. 2017), are a good climate dataset to validate the MPI with TCs modeled using the GCM. The d4PDF computed two different climate conditions using MRI-AGCM3.2H (an atmospheric GCM with horizontal 60-km resolution). The historical (or present) run is a 100 member ensemble of 60 years using an initial perturbation, and the future run is a 15 member initial ensemble using a 6 member SST ensemble run for 60 years. The total time integrations were 6000 years (60 years $\times$ 100 member) for the historical climate and 5400 years (60 years $\times$ 15 member $\times$ 6 sets) for the future climate condition. The future climate condition assumed a constant +4K degree warmer in the global mean ground temperature over the time periods. Specific details are found in (e.g., Ishii and Mori (2020)) and the application to storm surge projection is discussed in Mori et al. (2019a) and Ishii and Mori (2020).

We computed the MPI on a $1.25 \times 1.25^\circ$ grid with the monthly averaged data of the d4PDF dataset for both the historical and future climate conditions. The TCs are extracted based on SST, wind speeds, and other variables; they are used to adjust the TC genesis frequency in the historical run to augment the observed data (Yoshida et al. 2017). Here, we look at the probability density to analyze the relationship between the modeled TC pressure and the MPI, specifically, the relationship between the minimum central pressure below 950 hPa, $P_c^{\min}$, and the minimum MPI along its track, $\mathrm{MPI}_{\min}$ (Fig. 2).

Figure 2a shows the probability density function (pdf) of $\mathrm{MPI}_{\min}$ for both the historical and future climate runs. The relationship between the minimum central pressure of TC, $P_c^{\min}$, below 950 hPa and the minimum MPI, $\mathrm{MPI}_{\min}$, along its track is shown in Fig. 2. The pdf of $\mathrm{MPI}_{\min}$ is different between the present and future climate runs both weaker and stronger intensity. The pdf of $\mathrm{MPI}_{\min}$ in the future climate is wider than that in the present climate run. Figure 2b shows the difference between $P_c^{\min}$ and $\mathrm{MPI}_{\min}$ ($= P_{\mathrm{diff}}$). The negative value of P_{diff} means modeled TCs are developed and exceeded more than their MPI. The mean of P_{diff} in the present climate is 27.5 hPa and the standard deviation is 12.6 hPa. This means that the TC developed, on average, a minimum central pressure of up to +27.5 hPa for the MPI, and the error is roughly in the range of $\pm$12.6 hPa. The future climate has a smaller mean and smaller standard deviation for $P_c^{\min}$. The negative value means the developed TC exceeded its MPI.

The proportion of typhoons reaching their MPIs is 1.43 % in the present climate and 4.96 % in the future climate. This indicates that MPIs can generally estimate the maximum intensity of TCs in the climate model and 1–5% of TC can reached this ideal condition. More typhoons exceed the MPI in future climates than in present climates; this may be due to the future increase in areas with high SST in the north and the longer duration for TCs to track through the larger MPI environment, generally. However, we did not analyze the spatial difference between $P_c^{\min}$ and $\mathrm{MPI}_{\min}$ or the TC translation speed (Yamaguchi et al. 2020). These analyses are topics of further study of TC characteristics in future climate conditions.

3.2 Validation of the MPS model

The maximum sea surface deviation of the wind-induced surge using the cross-sectional topography along the bay axis is validated by dynamic storm surge simulations, first. Based

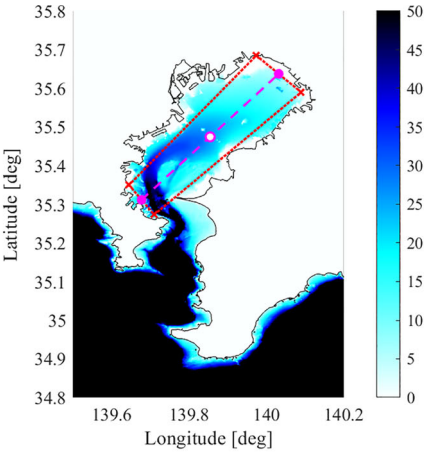

(a) Tokyo Bay

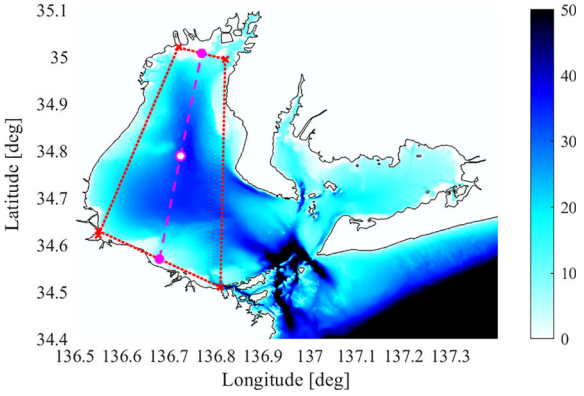

(b) Ise Bay

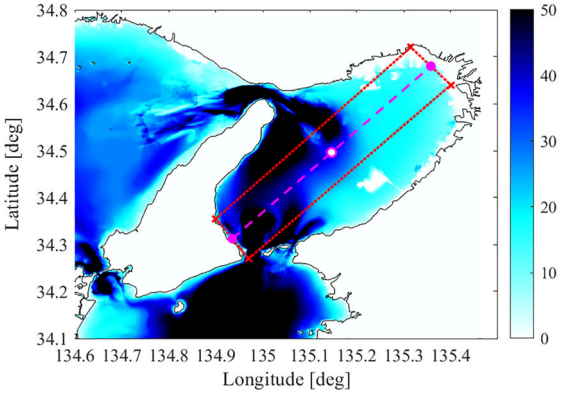

(c) Osaka Bay

Fig. 3 Definition of bay axis for target three bays (pink dashed line: the longest fetch, red dotted line: the simplified shape of the bay shape, filled circles: starting and ending points of the bay, open circle: middle of the bay, see cross sectional bathymetry along pink dashed line in Fig. A.1)

on Eq. 6, a series of numerical simulations is performed using topographic data for each bay. The coefficient K in Eq. 6 is tuned with the dynamic model results. Yasuda et al. (2016) computed a series of storm surge heights using the nonlinear shallow water equation (Kim et al. 2008) at three major highly populated bays in Japan (Tokyo, Osaka, and Ise Bays). The mean water depths of Tokyo, Osaka, and Ise Bays are 48.2 m, 49.1 m, and 54.5 m, respectively.

The computational conditions of the TCs approaching the three bays are forced with the climate projections by MRI-AGCM3.2H (Mizuta et al. 2012). The projections from MRI-AGCM3.2H use a 60-km horizontal resolution; 3 ensembles were performed for the present climate condition and 8 ensembles for future climate conditions. We used both climate conditions for validation. The performance of the climate model does not affect the accuracy of the MPS model itself once it satisfies the relation between Myers type pressure distribution and wind speed (see wind speed in Fujii and Mitsuta (1986) and TC radius in Kato (2005)). Using the climate projections, we obtained enough extreme events (275 years) to validate the model for each target bay to compare with historical events.

The comparison between the dynamic storm surge model and the MPS model is performed using the following conditions.

1. pick up storm surge events larger than 1 m
2. pick up minimum central pressures $P_{\min}$ and maximum wind speeds $V_{\max}$ from TCs in step 1
3. input $P_{\min}$ and $V_{\max}$ into the MPS model
4. compare maximum surge heights between dynamic model and MPS model

Figure 3 shows the central axis for Tokyo Bay; the pink dashed line indicates the longest fetch and the red dotted line illustrates the simplified shape of the bay. Figure A.1 shows the bathymetry and mean water depth along the longest fetch for each of the three bays. The shapes of the three bays are semi-enclosed, and therefore water flow into the bay is not significant. The bathymetry profiles at the bay mouths are not simple, but each profile monotonically decreases to the coastline except Ise bay. The different bathymetries give different degrees of accuracy between the constant depth model and the realistic bathymetry model. The different bathymetry profiles also needs different coefficient K in Eq. 6 and are tuned by the dynamic storm surge model.

First, the pressure-induced surge model is validated by selecting different TC translation speeds for all 225 cases. The difference between the numerical results and Eq. A.17 is small, with the largest difference of about 10 cm at most. The mean water depths for Tokyo, Osaka, and Ise Bays are 48.2 m, 49.1 m, and 54.5 m, respectively. Most of the TCs approaching Japan have long wave celerity values close to the model values for these three bays. In the following discussion, the assumed TC translation speed is close in value to the long wave velocity in each bay (e.g., 79 km/h).

Second, the wind-induced surge model is validated using the same dynamical model output. The results of the comparison between the dynamical model and the MPS model are based on the above procedure. The value of $V_{\max}$ is substituted into Eq. 6 and optimized for K. The K in Eq. 6 is optimized for cases having a wind angle parallel to bay of $\pm\pi/4$ to satisfy the longest fetch condition. The results of the dynamic model, however, were forced by different wind angles to the bays due to the arbitrary TC tracks.

The values of $P_{\min}$ and $V_{\max}$ are substituted into Eq. 6 with optimized K. Figure A.2 shows the comparison between the dynamic model and the MPS model of Eq. 6 forced by $P_{\min}$ and $V_{\max}$. The color of a data point in the figure indicates the clockwise angle with respect to the bay axis direction, with clockwise being positive (the longest fetch occurs at

0°). The MPS model assumes the case of the wind blowing parallel to the longest bay axis to estimate the maximum possible value, which corresponds to the range near 0°. As the MPS model is assumed the worst-case storm surge in which case storms travel along the longest fetch of the bay, Fig. A.2 indicates that the line $y = x$ corresponds almost the envelope of the plot. It shows that the maximum possible storm surge value for a given pressure and wind speed can be estimated using the MPS model. The RMSEs of the MPS model to the dynamic model for the samples ranged of angles from $\pm\pi/4$ are 0.05 m, 0.11 m, and 0.03 m for Tokyo Bay, Osaka Bay, and Ise Bay using Eq. 6, which is sufficient accuracy for such a simplified model for climatological application. On the other hand, the RMSEs of the MPS model with a constant water depth Eq. 5 to the dynamic model using a range of angles from $\pm\pi/4$ are 0.32 m, 0.35 m, and 0.71 m, respectively. Additionally, the R-squared values for the samples ranged of angles from $\pm\pi/4$ are 0.95, 0.66, and 0.95 for Tokyo Bay, Osaka Bay, and Ise Bay, respectively. The MPS model with real bathymetry using Eq. 6 gives enough accuracy for the worst-case storm surge. The MPS model can increase accuracy increasing number of teaching data.

In Ise Bay, the accuracy of surge height with Eq. 6 is significantly improved from that using Eq. 5. Ise Bay is a bowl-shaped basin with shallow water depths at the mouth and back of the bay, but Tokyo Bay and Osaka Bay have deep water at their entrances. Since the wind-surge effect is inversely proportional to the water depth, the wind surge is expected to be greater in shallower water depths. In Ise Bay, the wind-induced storm surge develops less than expected over the depth of the bay because the mouth of the bay on the bay axis is far from the connecting area. The influence of two-dimensional spreading is also strong, and the bathymetry of the bay is unlikely to be represented by the bay axis but more so by the shape of the bay. On the other hand, Tokyo or Osaka Bay are simple bays and the constant water depth assumption in Eq. 6 can be applied, which does not require integration of the equation numerically. In this procedure, we did not consider the location of the maximum water height; we will increase the number of cases and verify the accuracy by considering the location of the maximum water height.

The MPS model considers one-dimensional changes in depth using Eq. 6; it is simple to apply with no need for dynamic modeling procedures, yet it gives sufficient accuracy to estimate extreme storm surge heights given pressure values and wind speeds. Once $P_{\min}$ and $V_{\max}$ are estimated with the MPI model, it is possible to estimate the maximum potential surge height semi-empirically without a large computational load. A disadvantage of the MPS model is estimating the occurrence probability. With the assumptions of longest fetch and resonant TC translation speed, we cannot obtain probabilistic information using the MPS as we can with the MPI.

4 Projection of the MPI with the CMIP5 ensemble

The future trend of MPI change for each RCP scenario was analyzed using CMIP5. First, a sensitivity analysis of the MPI was performed considering the stability of the atmosphere. The differences between the present and future climates and between MPI and SST climates were analyzed for grid points with MPIs below 990 hPa in the tropics of the present climate for all months from January to December. The upper limit of the MPI for the current tropical climate is set because the input value of sea level pressure P_{env} of the environmental field, which is the input value of the MPI calculation, may be output as the MPI for environmental fields where typhoons are not sufficiently developed in the model. P_{env} is essentially

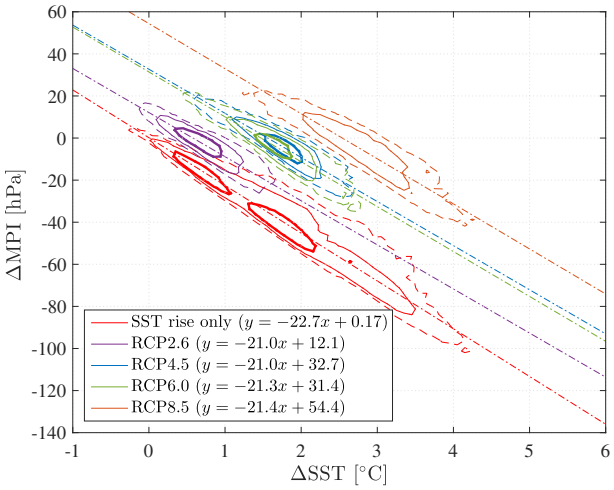

Fig. 4 Relationship of future change in SST ΔSST and MPI ΔMPI for HadGEM2-AO projection. (red: future SST only case of all RCPs, purple: RCP2.6, blue: RCP4.5, green: RCP6.0, orange: RCP8.5; contour by dashed line: 10 sample, solid line: 100 sample, bold line: 500 sample; single point chain: linear approximation)

uncorrelated to SST, and we prevented comparing two uncorrelated variables by setting an upper bound on MPI in the current climate.

The relationship between future changes in SST and MPI is shown in Fig. 4, which shows the case of GFDL-CM3 as an example. Figure 4 shows the contours of future change in SST, ΔSST, and MPI, ΔMPI, with the results from RCP2.6, 4.5, 6.0, and 8.5 indicated in purple, blue, green, and orange, respectively. The red lines in the figure show the case where only SST is taken into account for analysis of future climate, and the dashed-dot line shows a linear approximation of the results. The relationship between ΔSST and ΔMPI is linear, but different RCP scenarios have different intercepts depending on the emission scenario. The slopes of ΔSST/ΔMPI for the SST only case (red line) are −23 hPa/°C; it becomes −19 hPa/°C for the full calculation with the RCPs. This sensitivity range of MPI to SST agrees with the analysis of MPI to SST in JRA-55 reanalysis.

The higher emission scenarios show positive intercept values in ΔMPI. This means increasing atmospheric stability suppresses MPI intensity including ΔSST from increasing in those future climate conditions. Although MPI increased in response to the rise in SST in all RCP scenarios, the net increase in MPI in response to the SST increase is smaller in the higher RCP scenarios. As SST increases with warming, wetting is expected, especially in the lower troposphere near sea level, which reduces enthalpy fluxes at sea level and acts in weakening TC intensity (Tang and Emanuel 2010). The similar results of ΔSST and ΔMPI relation were obtained by the other 15 CMIP5 models except HadGEM2-AO with RCP4.5 and 6.0 scenarios. The mean sensitivity of MPI change per 1 degree SST in CMIP5 ensemble is about −23 hPa/°C in this analysis

Next we discuss the regional characteristics of MPI change that depend on latitude and season. The latitudinal distributions of the future change in MPI in September are shown in Fig. 5. In the figure, the marker indicates the monthly mean value, and the bar indicates the standard deviation. The different colors illustrate the different emission scenarios in the figure. The future change is latitude-dependent, with a clear increase in MPI at latitudes

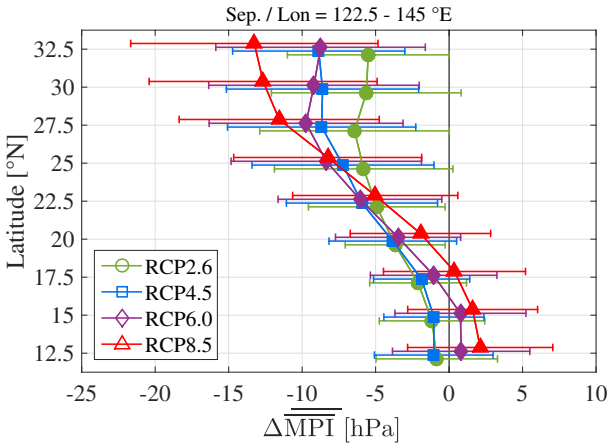

Fig. 5 Latitudinal distribution of future changes in MPI in September for each RCP scenario (markers: mean between GCMs, bars: standard deviation between GCMs)

above 25° N. The changes in MPI are significant for larger emission scenarios, showing both positive and negative changes. The largest changes in monthly mean MPI with RCP8.5 at 32° N is −13 hPa with about a 9 hPa standard deviation in September.

Since atmospheric stability will increase with warming as discussed in Fig. 4, Fig. 5 indicates neutral or weaker MPI changes in the lower latitudes (<15–20° N) where TC potential intensity is large enough in the present climate. The results are consistent with previous studies using d4PDF, such as Yoshida et al. (2017). Additionally, a similar analysis for future changes in SST indicates a linear change in the latitudinal direction because MPI-SST is correlated but is not a linear process. Therefore, the regional MPI changes are different from basin-averaged characteristics as shown in Fig. 4.

We analyzed seasonal changes of MPI in the middle latitudes (27.5–32.5° N, 122.5–145° E) for TCs targeting Japan in the WNP. The future change in MPI is shown for each month

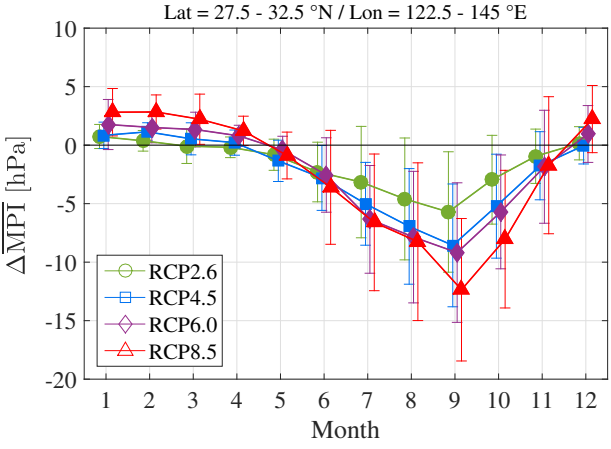

Fig. 6 Monthly change of future MPI change in the Pacific Ocean near Japan (marker: mean between GCMs, bar: standard deviation between GCMs)

in Fig. 6 and interpretation of the plot is similar to Fig. 5 except for monthly changes. The future MPI intensity increases the most in September, and a higher RCP scenario gives a larger future change. Particularly in September, the inter-GCM mean values are more than twice as high as those for RCP8.5 and RCP2.6 (−12.4 hPa and −5.7 hPa, respectively). On the other hand, the variation between the GCMs is large and is comparable to or larger than the difference between the RCP scenarios.

Finally, we analyzed future changes in MPI during the TC season in Osaka Bay based on current and future climates using 16 models from CMIP5 (see Fig. 7). The MPI was evaluated as the average of the four nearest points located south of each bay. Here we selected Osaka Bay but there is no significant difference between the three bays since they are located at a similar latitude in the WNP. The future change is the difference in local MPI from future to historical climates for each RCP for each month. From the left, each month from July to October is shown, and the results for RCP2.6 to RCP8.5 are shown in the plot for each of the months similar to the regional analysis. In September, the largest decrease in MPI can be observed from RCP8.5 in the same month that the intensity increases the most. The value of MPI decreases about −13 hPa with RCP8.5 in September, which correspond to the results shown in Fig. 5. The median value of changes in MPI shows the largest intensity increase with RCP8.5, but RCP8.5 has the largest range of uncertainty. The maximum value shows a decrease in intensity from RCP2.6 in some cases due to a signal to noise ratio. The RCP scenario and the temperature rise are positively correlated with each other, and this relationship includes noise due to a natural variability in the regional scale. The analyzed local MPI change takes into consideration for the analysis in MPS in the next section.

5 Projection of the MPS in the CMIP5 ensemble around Japan

Future changes in the MPS during the TC season are analyzed based on the historical and future climate conditions from 16 models of CMIP5. The future changes in MPS are shown in Fig. 8 as boxplots similar to the MPI boxplots shown in Fig. 7. As with the mean change in MPI, the height of mean MPS is the largest with RCP8.5 in the same month, September. The MPIs are similar in the bays because MPI is defined by large-scale environmental variables. MPS, however, is sensitive to local bathymetry; the averaged future changes in MPI for Osaka Bay, Ise Bay, and Tokyo Bay are 0.57, 0.41, and 0.40 m, respectively, for September with RCP8.5. The range of uncertainty is also very large, especially with RCP8.5 in July and August. There are many outliers, and the number of GCMs or ensemble sets needs to increase to estimate variability. Additionally, future changes in storm surge by MPS

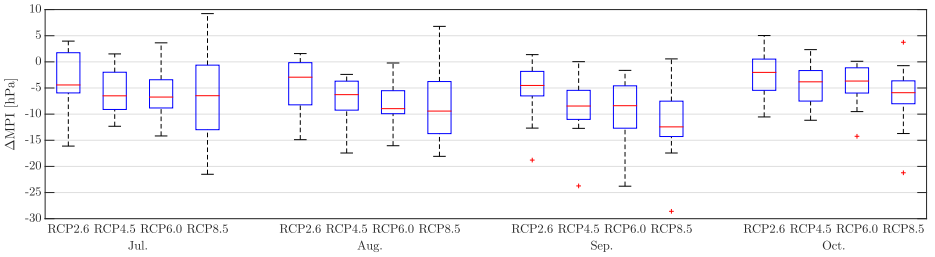

Fig. 7 Future changes in MPI in Osaka Bay (from left to right: July to October, by RCP scenario (red line: median, box: first and third quartiles, whiskers: maximum and minimum, +: outlier)

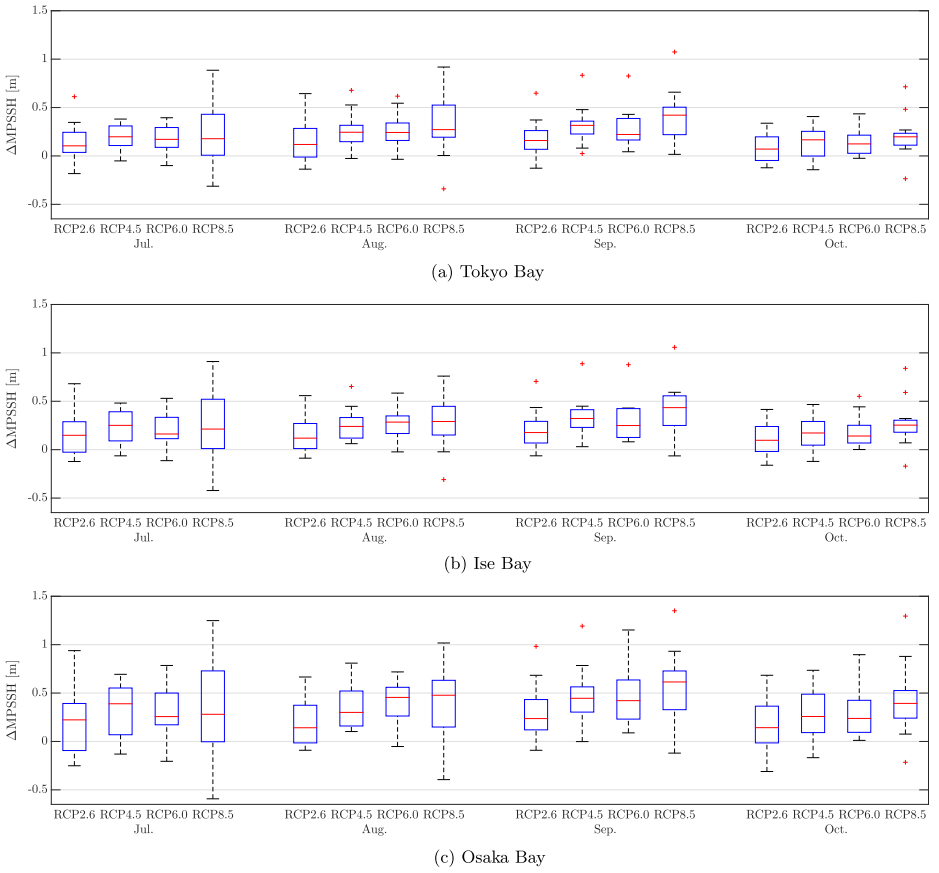

Fig. 8 Future changes in maximum potential storm surge height (MPS) for the three major bays: from left to right, July to October, for each RCP scenario (red line: median, box: first and third quartiles, whiskers: maximum and minimum, +: outliers, maximum whisker length is 1.5 times the quartile range)

in Osaka indicate increase storm surge heights as 0.57 m, 0.67 m, and 0.87 m by mean, mean plus 1σ, and mean plus 3σ cases in RCP8.5 in September which are large enough to consider adaptation strategy in comparison with projected sea level rise (0.84 m global mean). Although we cannot estimate probability of MPS in this analysis, these values are significant to know as a good step of local impact assessment in the coastal zone.

Next, the sensitivity of the storm surge anomaly to MPI is examined to understand impact of SST change in local extreme storm surge height using the MPI values from Figs. 7 and 8. There is no significant differences between August and September. The boxplot of ΔMPS/ΔSST for each bay and RCP is shown in Fig. 9. The sensitivity of SST to MPS for RCP8.5 at Tokyo Bay is 0.12 m/°C on average, and its standard deviation is 0.1 m/°C in September. The sensitivity of SST to MPS increases from Tokyo Bay to Ise Bay to Osaka Bay due to the bathymetric influence on wind-induced surge effects. The sensitivity of SST to MPS tends to decrease for higher RCP scenarios. The higher the RCP scenario, the smaller the value when ΔMPS is divided by ΔSST, because the higher the RCP scenario, the larger the increase in SST relative to the increase in MPS. The reason for this relatively

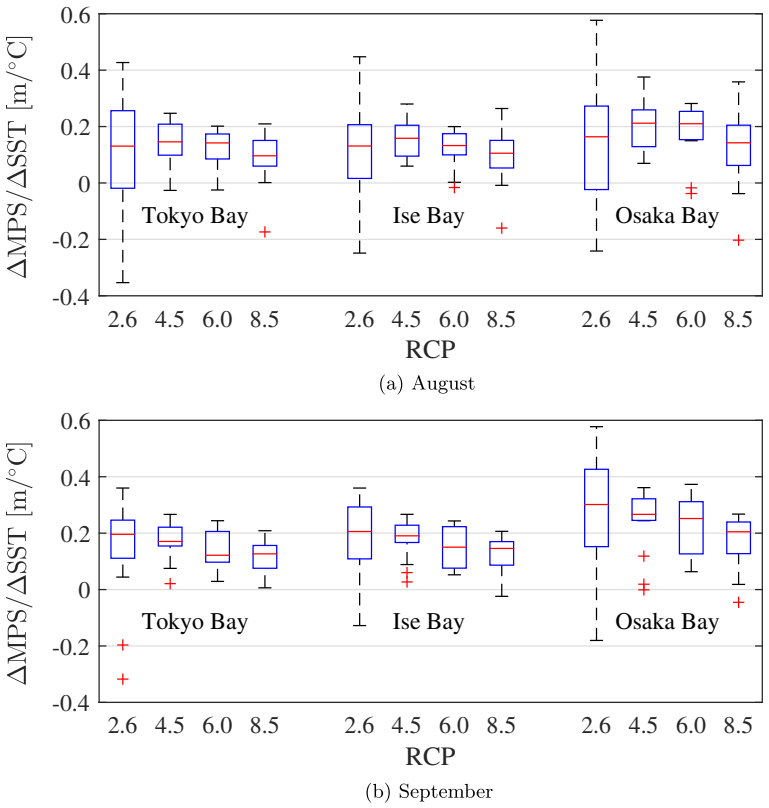

Fig. 9 Relation between changes in ratio of MPS/SST for the three major bays: from left to right, Tokyo to Osaka, for each RCP scenario (red line: median, box: first and third quartiles, whiskers: maximum and minimum, +: outliers, maximum whisker length is 1.5 times the quartile range)

small increase of MPS relative to SST is that the increase in atmospheric temperature is also larger and the atmospheric stability also increases. For RCP2.6, the median of the ratio ΔMPS/ΔSST is smaller than for the other RCPs during some months, because there are more models with negative ΔMPS in RCP2.6 than with the other RCPs. Since ΔSST is positive in all models, the resulting ΔMPS/ΔSST ratio is negative in more models than other RCPs, where the median value decreases.

These results confirm that the change in SST is the largest with RCP8.5 in East Asia region in the month of September. However, the increase in storm surge height per 1 °C rise in SST is the largest with RCP2.6.

6 Conclusion

In this study, a simple and seamless method to estimate the potential maximum storm surge height (MPS) was developed to project future changes in the extreme storm surge height using the theory of maximum potential intensity (MPI) of a tropical cyclone (TC). A simplified storm surge model that considers the cross-sectional bathymetry of a bay was introduced to the MPS model. It is possible to evaluate the maximum potential storm surge

height while maintaining a minimum of accuracy. The model was applied to CMIP5 models in the Western North Pacific considering several emission scenarios and analyzed by season. The main results are summarized as follows.

1. The MPI can generally estimate the top 10% of TCs by intensity in the global climate model
2. The changes in MPI depend on the increasing SST and atmospheric stability effect. MPI becomes larger for higher RCP scenarios.
3. The changes in MPI become significant in the middle latitudes in September. The mean increases of MPI are −12.4 hPa and −5.7 hPa for the RCP8.5 and RCP2.6 scenarios.
4. The sensitivity of MPS changes to SST changes during the TC season in the three major bays in Japan averaged about 0.12 m/°C.
5. In future climates, MPS is expected to increase significantly in both mean and variance, especially in September, and the change is larger as the RCP scenario becomes higher.

Several analysis remains to be explored. This model can also be applied to other ocean basins, and we will consider the occurrence probability of storm surge using MPS in the future.

Supplementary Information The online version contains supplementary material available at (https://doi.org/10.1007/s10584-021-02980-x).

Acknowledgements We appreciate for three anonymous reviewers for valuable comments.

Funding This work was conducted under the framework of the Integrated Research Program for Advancing Climate Models (TOUGOU Program, Grant Number JPMXD0717935498) supported by the Ministry of Education, Culture, Sports, Science, and Technology-Japan (MEXT) and the JSPS Grant-in-Aid for Scientific Research (KAKENHI).

References

Balaguru K, Judi DR, Leung LR (2016) Future hurricane storm surge risk for the US gulf and Florida coasts based on projections of thermodynamic potential intensity. Clim Chang 138:99–110

Bender MA, Knutson TR, Tuleya RE, Sirutis JJ, Vecchi GA, Garner ST, Held IM (2010) Modeled impact of anthropogenic warming on the frequency of intense Atlantic hurricanes. Science 327:454–458

Bloemendaal N, Muis S, Haarsma RJ, Verlaan M, Apecechea MI, de Moel H, Ward PJ, Aerts JCJH (2019) Global modeling of tropical cyclone storm surges using high-resolution forecasts. Clim Dyn 52:5031–5044

Emanuel KA (1988) The maximum intensity of hurricanes. J Atmos Sci 45:1143–1155

Emanuel KA (2013) Downscaling CMIP5 climate models shows increased tropical cyclone activity over the 21st century. Proc Natl Acad Sci 110:12219–12224

Fujii T, Mitsuta Y (1986) Simulation of winds in typhoons by a stochastic model. Wind Engineers JAWE 1986:1–12

IPCC WGI (2013) Climate change 2013: the physical science basis: working group I contribution to the fifth assessment report of the Intergovernmental Panel on Climate. Change IPCC WGI. Accessed May 14 2014

Irish JL, Resio DT, Cialone MA (2009) A surge response function approach to coastal hazard assessment. Part 2: Quantification of spatial attributes of response functions. Nat Hazards 51:183–205

Ishii M, Mori N (2020) d4PDF: Large-ensemble and high-resolution climate simulations for global warming countermeasures. Progress in Earth and Planetary Science https://doi.org/10.1186/s40645–020–00367–7

Ishii M, Shouji A, Sugimoto S, Matsumoto T (2005) Objective analyses of sea-surface temperature and marine meteorological variables for the 20th century using ICOADS and the Kobe collection. Int J Climatol A J R Meteorol Soc 25:865–879

Kato F (2005) Study on risk assesment of storm surge flood. Technical note of National Institute for Land and Infrastructure Management

Kim SY, Yasuda T, Mase H (2008) Numerical analysis of effects of tidal variations on storm surges and waves. Appl Ocean Res 30:311–322

Knutson TR, McBride JL, Chan J, Emanuel K, Holland G, Landsea C, Held I, Kossin JP, Srivastava AK, Sugi M (2010) Tropical cyclones and climate change. Nat Geosci 3:157–163

Kobayashi S, Ota Y, Harada Y, Ebita A, Moriya M, Onoda H, Onogi K, Kamahori H, Kobayashi C, Endo H, et al. (2015) The JRA-55 reanalysis: general specifications and basic characteristics. J Meteorol Soc Japan Ser II(93):5–48

Lin N, Marsooli R, Colle BA (2019) Storm surge return levels induced by mid-to-late-twenty-first-century extratropical cyclones in the Northeastern United States. Clim Chang 154:143–158

Mizuta R, Murata A, Ishii M, Shiogama H, Hibino K, Mori N, Arakawa O, Imada Y, Yoshida K, Aoyagi T et al (2017) Over 5,000 years of ensemble future climate simulations by 60-km global and 20-km regional atmospheric models. Bull Am Meteorol Soc 98:1383–1398

Mizuta R, Yoshimura H, Murakami H, Matsueda M, Endo H, Ose T, Kamiguchi K, Hosaka M, Sugi M, Yukimoto S, et al. (2012) Climate simulations using MRI-AGCM3. 2 with 20-km grid. J Meteorol Soc Japan Ser II(90):233–258

Mori N, Kato M, Kim S, Mase H, Shibutani Y, Takemi T, Tsuboki K, Yasuda T (2014) Local amplification of storm surge by Super Typhoon Haiyan in Leyte Gulf. Geophys Res Lett 41:5106–5113

Mori N, Tomoya S, Kohei Y, Ryo M, Yasuko O, Mikiko F, Temur K, Eiichi N (2019a) Future changes in extreme storm surges based on mega-ensemble projection using 60-km resolution atmospheric global circulation model. Coastal Eng J 61:295–307

Mori N, Takemi T (2016) Impact assessment of coastal hazards due to future changes of tropical cyclones in the North Pacific Ocean. Weather Clim Extremes 11:53–69

Mori N, Yasuda T, Arikawa T, Kataoka T, Nakajo S, Suzuki K, Yamanaka Y, Adrean W (2019b) 2018 Typhoon Jebi post-event survey of coastal damage in the Kansai region, Japan. Coastal Eng J 61:278–294

Nakajo S, Mori N, Yasuda T, Mase H (2014) Global stochastic tropical cyclone model based on principal component analysis and cluster analysis. J Appl Meteorol Climatol 53:1547–1577

Pörtner HO, Roberts D, Masson-Delmotte V, Zhai P, Tignor M, Poloczanska E, Mintenbeck K, Nicolai M, Okem A, Petzold J, et al. (2019) IPCC special report on the ocean and cryosphere in a changing climate IPCC intergovernmental panel on climate change. Geneva, Switzerland

Proudman J (1929) The effects on the sea of changes in atmospheric pressure. Geophys Suppl Mon Notices Royal Astron Soc 2:197–209

Schiermeier Q (2013) Did climate change cause typhoon haiyan? nature news

Tang B, Emanuel K (2010) Midlevel ventilation's constraint on tropical cyclone intensity. J Atmos Sci 67:1817–1830

Yamaguchi M, Chan JCL, Moon IJ, Yoshida K, Mizuta R (2020) Global warming changes tropical cyclone translation speed. Nat Commun 11:1–7

Yasuda Tomohiro, Yamamoto Yusuke, Mori Nobuhto, Mase Hajime (2016) Future change projections of storm surge using MRI-AGCM3.2h ensemble. J Japan Soc Civil Eng Ser. B2 (Coastal Eng) 72:I1477–I1482

Yoshida K, Sugi M, Mizuta R, Murakami H, Ishii M (2017) Future changes in tropical cyclone activity in high-resolution large-ensemble simulations. Geophys Res Lett 44:9910–9917